Performance evaluation of FFT_PCA Method based on dimensionality reduction algorithms in improving classification accuracy of OLI data

Parviz Zeaiean Firooz Abadi[a*], Hasan Hasani Moghaddam[b]

[a] *Associated professor of remote sensing and GIS, Faculty of Geography, Kharazmi University*
[b] *MA of remote sensing and GIS, Kharazmi University*

Abstract

Fusions of panchromatic and multispectral images create new permission to gain spatial and spectral information together. This paper focused on hybrid image fusion method FFT-PCA, to fuse OLI bands to apply Dimensionality Reduction (DR) methods (PCA, ICA and MNF) on this fused image to evaluate the effect of these methods on final classification accuracy. A window of OLI images from Ardabil County was selected to this purpose and preprocessing method like atmospheric and radiometric correction was applied on this image. Then panchromatic (band8) and multispectral bands of OLI were fused with FFT-PCA method. Three dimensionality reduction algorithms were applied on this fused image and the training data for classification were selected from DRs Output. A total of eight classes include bare land, rich range land, water bodies, settlement, snow, agricultural land, fallow and poor range land were selected and classified with support vector machine algorithm. The results showed that classification based on dimensionality reduction algorithms was quite good on OLI data classification. Overall accuracy and kappa coefficient of classification images showed that ICA, PCA and MNF methods 86.9%, 89%, 96.8% and 0.84, 0.91, 0.96 respectively. The MNF based image classification has higher classification accuracy between two others. PCA and ICA have lower accuracy than MNF respectively.

Keywords: Hybrid fusion, FFT-PCA, Dimensionality reduction algorithms, Support vector machine.

---

* Corresponding author. Tel: +98-9123903621.
 E-mail address: zeaiean@khu.ac.ir.

1. Introduction

Remote sensed data have been used to extract relevant information on various natural recourses and environments (Kumar Singla et al., 2018). Land cover is critical information to various land management and scientific application (Liu, 2017). There are large numbers of methods developed and applied to increase total accuracy of land use/cover mapping from satellite imagery (Hasani Moghaddam et al., 2018). Fusion of panchromatic and multispectral bands, is the most critical way to increase information extraction accuracy (Vivekan et al., 2014; Unlusoy, 2013). In recent years, Hybrid image fusion methods were implemented for the fusion of multi resolution images (Dhavan and Garg, 2014). PCA+SWT (Kaur, 2016), DDCT+PCA (Mamachan and Baby, 2015), FFT-HIS (Yusuf et al., 2013), and FFT-PCA (Bashirpour et al., 2017), Are the most important hybrid methods that have been used in recent researches. One of the most effective hybrid methods is FFT_PCA that also preserve spectral and spatial information of the multispectral and panchromatic images as well as original inputs (Bai et al., 2015). The reduction of the dimension of fused image is an important way to perform faster classification. The dimensionality reduction algorithms can efficiently brought down the data to a much smaller number of variables without a significant loss of information (Sorzano et al., 2014). PCA is one of the effective dimensionality reduction methods that tries to find a new coordinate system in which the input data can be expressed with many less variables without a significant error (Sorzano et al., 2014). Another method for dimensionality reduction (DR) is MNF that provides a linear transformation of data, in which the noise data values are lower in the initial conversions, and the amount of noise increases further components (Hasani Moghaddam, 2017). The ICA DR method has received considerable interest in recent years. The key idea of ICA assumes that data are linearly mixed with a set of separate independent sources and demix this signal sources according to their statistical independent measured by mutual information (Wang and Chang, 2006).

Wang and Chang (2006), worked on application of independent analysis in hyper spectral images. The study illustrates that ICA dimensionality reduction methods uses mutual information as a criterion to measure data statistical independency that exceeds second order statistics. The results of the study showed that ICA-DR provide advantages over the PCA-DR and MNF-DR.

Sahisi and Krishna (2016) have done researches in performance evaluation of dimensionality reduction techniques on CHRIS hyper spectral data for surface discrimination title. In this study, they used MNF, PCA and ICA DR methods. They used Hybrid dimensionality reduction method for extracting the concrete materials from the CHRIS hyper spectral data. SAM and SID classifier were used to classify surface materials. The results showed that, SAM classifier gave the best results with an accuracy improvement of 10% after adapting the hybrid method.

Arslan et al., (2017), compared performance of classification methods for a hyper spectral images data set in view of dimensionality reduction methods. Among the DR methods, ICA, PCA and MNF were used in this study. Four classification algorithms including MLC, MD, SAM and SVM were used to evaluate more accurate method among them. The results showed that MLC algorithm

generally performed better than the other classifier while the SAM exhibited significantly lower accuracies in the experiments.

Wang and chang(2017), have studied on unsupervised feature extraction for hyper spectral images by using combination low rank representation and locally linear embedding. They used MNF, PCA and ICA methods for dimensionality reduction of data. The results showed that the PCA method has better performance by 0.77 kappa coefficient and ICA has lower performance by 0.70 kappa coefficient.

The aim of this study is to fused panchromatic and multispectral OLI bands with FFT_PCA method and then apply DR algorithms to this fused image to evaluate the effect of these DR methods on Support Vector Machine of OLI classification accuracy.

2. Material and Methods

2.1. Study area

An area of 2565.838 square kilometer, in Ardabil county is located between 37.45- 39.42 northing latitudes and 47.30-48.55 easting longitudes at northwest of Iran (Ghasemlounia and Sedaghat Herfe, 2017). In this region, the lowest elevation in Ardebil plain is 1294 meters and the highest elevation (Sabalan peak) is 4811 meters above sea level. The average rainfall and annual temperature are 318.4 mm and 14.87°C respectively (Torahi et al., 2016). Figure (1), shows the geographic location of Ardabil county.
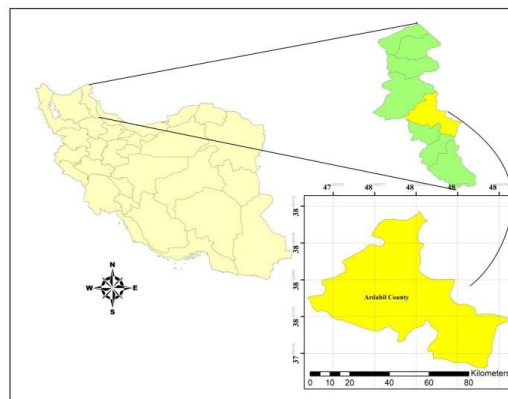
figure 1. Geographic location of study area

2.2. Satellite data used

The OLI sensor provides nine spectral bands (1-9) and TIRS provides two spectral bands (10-11), as shown in Table 1. Seven bands from band 2 to band 7 of OLI are consistent with the TM and ETM+ sensors. The new two spectral bands, band 1 and band 9 allow measuring water resources and coastal zone investigation and improving the detection of cirrus clouds. TIRS conducts thermal

imaging which can be applicable to evapotranspiration rate measure for water management (Chul ko et al., 2015).

Table 1. Wavelength and spatial resolution of the Landsat 8 OLI and TIRS (Knight and Kvaran, 2014 ; Alhirmizy, 2015)

Band	Wavelength Range(μm)	Spatial resolution(m)
OLI 1	0.433-0.453 (Coastal/aerosol)	30
OLI 2	0.450-0.515 (blue)	30
OLI 3	0.525-0.600 (green)	30
OLI4	0.630-0.680 (green)	30
OLI 5	0.845-0.885 (Near-IR)	30
OLI 6	1.560-1.660 (SWIR-1)	30
OLI 7	2.100-2.300(SWIR-2)	30
OLI 8	0.500-0.680 (Pan)	15
OLI 9	1.360-1.390 (Cirrus)	30
TIRS 10	10.30-11.30 (LWIR-1)	100
TIRS 11	11.50-12.50 (LWIR-2)	100

2.3. Methods

The image of Landsat 8-OLI were downloaded from USGS explorer and some image preprocessing analysis such as atmospheric and radiometric corrections were performed on the image before fusing panchromatic and multispectral bands. The FFT-PCA method was used to fuse OLI bands to get 15 meter resolution. Then three DR methods including PCA, ICA and MNF were performed on this fused image and results were classified with Support Vector Machine (SVM) algorithm. The performance of each DR algorithms was evaluated to improve the accuracy of classification of final images using overall accuracy and Kappa coefficient.

2.3.1. Principal Component Analysis (PCA)

PCA is a common technique for DR and finding pattern in high dimension data, Proposed by Pearson in 1901. It is based on computation of low-dimensional representation of a high-dimensional dataset that maximizes the total distribution which is optimal in reconstruction (Ping et al., 2017). The following describes the description in steps:

Step 1. The m samples can be represented by a set of $\Psi = \{X_1, X_2, ..., X_m\}$. For each sample, which has n indicators, it can be described as $\Psi = \{X_1, X_2, ..., X_m\}$ for $i \in \{1, 2, ..., m\}$, and then a m*n matrix X can be constructed with all the observation as follows:

$$X = \begin{bmatrix} X_1 \\ X_2 \\ \vdots \\ X_m \end{bmatrix} = \begin{bmatrix} X_{11} & X_{12} & \cdots & X_{1n} \\ X_{21} & X_{22} & \cdots & X_{2n} \\ \vdots & \vdots & \vdots & \vdots \\ X_{m1} & X_{m2} & \cdots & X_{mn} \end{bmatrix}. \tag{1}$$

Then based on Matrix X, the standardized matrix X* can be obtained by the following procedure.

$$
X^* = \begin{bmatrix} X^*_1 \\ X^*_2 \\ \vdots \\ X^*_m \end{bmatrix} = \begin{bmatrix} X^*_{11} & X^*_{12} & \cdots & X^*_{1n} \\ X^*_{21} & X^*_{22} & \cdots & X^*_{2n} \\ \vdots & \vdots & \vdots & \vdots \\ X^*_{m1} & X^*_{m2} & \cdots & X^*_{mn} \end{bmatrix} \tag{2}
$$

Where $X^*_i = (x^*_{i1}, x^*_{i2}, \ldots x^*_{in})$, $x^*_{ij} = (x_{ij} - \bar{x}_j)/\sqrt{var(x_j)}$ is the value of the element in the X* after standardizing, $\bar{x}_{ij} = (1/n)\sum_i^n = 1 x_{ij}$ and $var(x_j) = (1/(n-1))\sum_i^n = 1(x_{ij} - \bar{x}_j)^2$ is the average value and the variance of the jth column of matrix X respectively, for $i \in \{1, 2, \ldots, m\}$ and $j = \{1, 2, \ldots, n\}$.

Step 2. Therefore, the correlation matrix R based on the matrix X* can be obtained.

$$
R = \begin{bmatrix} r_{11} & r_{12} & \cdots & r_{1n} \\ r_{21} & r_{22} & \cdots & r_{2n} \\ \vdots & \vdots & \vdots & \vdots \\ r_{n1} & r_{n2} & \cdots & r_{nn} \end{bmatrix} \tag{3}
$$

Where the value of element r_{ij} in the matrix R can be calculated as follows:

$$
r_{ij} = \frac{\sum_k^m = 1(x^*_{ki} - \bar{x}^*_i)(x^*_{kj} - \bar{x}^*_j)}{\sqrt{\sum_k^m = 1(x^*_{ki} - \bar{x}^*_i)^2 \sum_k^m = 1(x^*_{kj} - \bar{x}^*_j)^2}} \tag{4}
$$

Where $\bar{x}^*_i$, $\bar{x}^*_i = (1/n)\sum_j^n = 1 x^*_{ij}$, for $i \in \{1, 2, \ldots, n\}$ and $j \in \{1, 2, \ldots, n\}$.

Step 3. The n eigenvalues $\lambda_1 \geq \lambda_2 \geq \ldots \geq \lambda_n > 0$ of matrix R and the corresponding n eigenvectors $a_1, a_2, \ldots, a_n$ can be obtained,

$$
a_1 = \begin{bmatrix} a_{11} \\ a_{21} \\ \vdots \\ a_{n1} \end{bmatrix} \quad a_2 = \begin{bmatrix} a_{12} \\ a_{22} \\ \vdots \\ a_{n2} \end{bmatrix}, \quad a_n = \begin{bmatrix} a_{1n} \\ a_{21} \\ \vdots \\ a_{m} \end{bmatrix} \tag{5}
$$

N principal components is obtained:

$$F_i = a_{1i} \times X^*_1 + a_{2i} \times X^*_2 + \dots + a_{ni} \times X^*_m \,, (i = 1, 2, \dots, n) \,. \qquad (6)$$

Step 4. Compute the contribution rate CR_i and the accumulative contribution rate ACR_i of each principal component $F_i \, (i = 1, 2, \dots, n)$, respectively:

$$CR_i = \frac{\lambda_i}{\sum_{k=1}^{n} 1^{\lambda k}} \,,$$

$$ACR_i = \sum_{k=1}^{i} CR_k \qquad (7)$$

Usually the top t principal components are retained. $F_1 F_2, \dots, F_t$, which correspond to the eigenvalues $\lambda_1, \lambda_2, \dots, \lambda_t$, and the corresponding accumulated contribution rate should satisfy that $ACR - t \geq 85\%$.

Step 5. Through plugging the elements in the matrix X* into the expression of t principal components, the score matrix F can be obtained.

$$F = \begin{bmatrix} F_{11} & F_{12} & \cdots & F_{1t} \\ F_{21} & F_{22} & \cdots & F_{2t} \\ \vdots & \vdots & \vdots & \vdots \\ F_{m1} & F_{m2} & \cdots & F_{mt} \end{bmatrix}, \qquad (8)$$

Where $F_{ij} = a_{1j} x^*_{j1} + a_{2j} x^*_{j2} + \dots + a_{ni} x^*_{jn}$ for $i \in \{1, 2, \dots, m\}$ and $j \in \{1, 2, \dots, t\}$.

Therefore, the original matrix X has been transformed into matrix F that has reduced dimensionally, while not losing much information of the original data.

Step 6. The score matrix F= $\left[F_{ij} \right] m \times t$ is a $m \times t$ matrix, the ith samples total points (TP), $TP_i = \sum_{j=1}^{t} 1 \, F_{ij} \times CR_j$ can be obtained, where CR_j is the jth eigenvalues contribution rate.

2.3.2. Fast Fourier Transform

The Fast Fourier Transform (FFT) is used as a noise reduction mechanism during image processing. The FFT is a computational efficient algorithm used to compute the Discrete Fourier Transform (DFT) and its inverse (IDFT). The FFT algorithm reduces the computational burden to (ONlogN) arithmetic operations. The FFT is a computational efficient method of generating a Fourier transform (Asiedu et al., 2016).

The first stage in execution of FFT during image processing is to compute the Discrete Fourier Transform. The DFT of a column vector, m_{jk} is represented mathematically as:

$$m^*_{jk} = DFT \{ m_{jk} \} = \sum_{r=0}^{p-1} m_{jk} e^{-i(2\pi s r / p)}, \qquad (9)$$

Where $s = 0, 1, \dots, p - 1, j = 1, 2, \dots, n$ and $i = \sqrt{-1}$.

Where m_{jk} is the kth column of the image matrix. For an image matrix of order 4, $p = 4$ and $s = 0, 1, 2, 3$. The DFT becomes;

$$m*_{j0k} = m_{j0k}e^{-0.ip/2} + m_{j1k}e^{-0.ip/2} + m_{j2k}e^{-0.ip/2} + m_{j3k}e^{-0.ip/2},$$

$$m*_{j1k} = m_{j0k}e^{-0.ip/2} + m_{j1k}e^{-1.ip/2} + m_{j2k}e^{-2.ip/2} + m_{j3k}e^{-3.ip2},$$

$$m*_{j2k} = m_{j0k}e^{-0.ip/2} + m_{j1k}e^{-2.ip/2} + m_{j2k}e^{-4.ip/2} + m_{j3k}e^{-6.ip/2},$$

$$m*_{j3k} = m_{j0k}e^{-0.ip/2} + m_{j1k}e^{-3.ip2} + m_{j2k}e^{-6.ip/2} + m_{j3k}e^{-9.ip/2}.$$

(10)

Therefore,

$$\begin{bmatrix} m*_{j0k} \\ m*_{j1k} \\ m*_{j2k} \\ m*_{j3k} \end{bmatrix} = \begin{bmatrix} e^{-0.i\pi/2} & e^{-0.i\pi/2} & e^{-0.i\pi/2} & e^{-0.i\pi/2} \\ e^{-0.i\pi/2} & e^{-1.i\pi/2} & e^{-2.i\pi/2} & e^{-3.i\pi2} \\ e^{-0.i\pi/2} & e^{-2.i\pi/2} & e^{-4.i\pi/2} & e^{-6.i\pi/2} \\ e^{-0.i\pi/2} & e^{-3.i\pi2} & e^{-6.i\pi/2} & e^{-9.i\pi/2} \end{bmatrix} \begin{bmatrix} m_{j0k} \\ m_{j1k} \\ m_{j2k} \\ m_{j3k} \end{bmatrix}$$

(11)

And

$$\begin{bmatrix} m*_{j0k} \\ m*_{j1k} \\ m*_{j2k} \\ m*_{j3k} \end{bmatrix} = \begin{bmatrix} 1 & 1 & 1 & 1 \\ 1 & -i & -1 & i \\ 1 & -1 & 1 & -1 \\ 1 & i & -1 & -i \end{bmatrix} \begin{bmatrix} m_{j0k} \\ m_{j1k} \\ m_{j2k} \\ m_{j3k} \end{bmatrix}$$

(12)

The next stage is to compute the Inverse Discrete Fourier Transform (IDFT). The IDFT is given by:

(13)

$$m_{jk} = IDFT\{m*_{jk}\} = \frac{1}{p}\sum_{r=0}^{p-1} m*_{jk}e^{i(2\pi sr/p)},$$

For $p = 4$ the IDFT is giv

$$\begin{bmatrix} m_{j0k} \\ m_{j1k} \\ m_{j2k} \\ m_{j3k} \end{bmatrix} = \frac{1}{4}\begin{bmatrix} e^{-0.i\pi/2} & e^{-0.i\pi/2} & e^{-0.i\pi/2} & e^{-0.i\pi/2} \\ e^{-0.i\pi/2} & e^{-1.i\pi/2} & e^{-2.i\pi/2} & e^{-3.i\pi2} \\ e^{-0.i\pi/2} & e^{-2.i\pi/2} & e^{-4.i\pi/2} & e^{-6.i\pi/2} \\ e^{-0.i\pi/2} & e^{-3.i\pi2} & e^{-6.i\pi/2} & e^{-9.i\pi/2} \end{bmatrix} \begin{bmatrix} m*_{j0k} \\ m*_{j1k} \\ m*_{j2k} \\ m*_{j3k} \end{bmatrix}$$

(14)

And

$$\begin{bmatrix} m_{j0k} \\ m_{j1k} \\ m_{j2k} \\ m_{j3k} \end{bmatrix} = \frac{1}{4}\begin{bmatrix} 1 & 1 & 1 & 1 \\ 1 & i & 1 & -i \\ 1 & 1 & -1 & 1 \\ 1 & -i & 1 & i \end{bmatrix} \begin{bmatrix} m*_{j0k} \\ m*_{j1k} \\ m*_{j2k} \\ m*_{j3k} \end{bmatrix}$$

(15)

2.3.3. Independent Component Analysis

Independent component analysis (ICA) is a multivariate data analysis method that, gives a linear mixture of statistical independent sources and recovers these components by producing an unmixing matrix (Varshney and Arora, 2004). A problem setting of ICA is as follows: Assume there is an L_ dimensional Zero_ mean non Gaussian source vector $s(n) = [s_1(n), ..., s_L(n)]^T$, such that the components $S_i(n)'s$ are mutually independent and an observed data vector $x(n) = [x_1(n), ..., x_N(n)]$ is composed of linear combination of sources $S_i(n)$ at each time point n, such that

$$X(n) = As(n) \tag{16}$$

Where A is a full rank $N \times L$ matrix where $L \leq N$. The goal of ICA is to find a linear mapping W such that each component of an estimate u of the source vector Is independent as possible.

$$u(n) = Wx(n) = WAs(n) \tag{17}$$

The original sources s (n), are exactly recovered when W is the pseudo_ inverse of A up to some scale changes and permutations. For a derivation of an ICA algorithm, one usually assumes that L=N, because there is no idea about the number of sources. In addition, sources are assumed to be independent of time n and are drawn from independent identical distribution $p_i(s_i)$ (Kawn and Kim, 2006).

2.3.4. Minimum Noise Fraction

Minimum noise fraction (MNF) is a well-known technique for hyper spectral imagery denoising. It transforms a noisy data cube into output channel images with steadily increasing noise levels, which means that the MNF output images contain steadily decreasing image quality (Lou et al., 2016). In a common practice, MNF components with eigenvalue less than 1 such as noise are usually excluded from the data in order to improve the subsequent spectral processing results, since Eigen images with near unity eigenvalues are normally noise dominated (Qiu et al., 2006).

3. Classification

After applying FFT-PCA method on OLI bands, three dimensionality reduction algorithms (PCA, ICA, MNF) applied on this fused image and regarding field surveys and visual interpretation of the images, a total of 8 classes including water bodies, snow, rich range lands, poor range lands (degraded), agricultural lands, fallow, bare lands and settlement were selected and training data of each other were taken from the images. A total of 150 training samples for each class were selected from the images after applying the FFT-PCA-PCA, FFT-PCA-ICA and FFT-PCA-MNF methods. After using this method, the separability of the samples was evaluated using the Jeffris Matusita index.

Support vector machine is a useful technique for data classification (Abbasi et al., 2015). A classification task usually involves separating data into training and testing sets. Each instance in the training set contains one "target value" (i.e. the class labels) and several "attributes" (i.e. the features or observed variables). The goal of SVM is to produce a model (based on the training data) which predicts the target values of the test data given only the test data attributes (Hsu et al., 2003).

Given a training set of instance label point $(x_i, y_i), i = 1, ..., l$ where $x_i \in R^n$ and $y \in \{1, -1\}^l$, the support vector machine (SVM) requires the solution of the following optimization problem:

$$\min_{w, b, \epsilon} \quad \frac{1}{2} w^T w + C \sum_{i=1}^{l} \epsilon_i$$

$$\text{Subject to } y_i (w^T \phi(x_i) + b) \geq 1 - \epsilon_i, \tag{18}$$

$$\epsilon_i \geq 0.$$

Here the training vector xi is mapped into a higher (maybe infinite) dimensional space by the function ϕ. SVM finds a linear separating hyperplane with the maximal margin in this higher dimensional space. $C > 0$ is the penalty parameter of the error term. Furthermore, $K(x_i, x_j) = \phi(x_i)^T \phi(x_j)$ is called the kernel function. Though new kernels are being proposed by researchers, beginners may find in SVM books the following four basic kernels:

- Linear: $K(x_i, x_j) = x_i^T x_j$.

- Polynomial: $K(x_i, x_j) = (\gamma x_i^T x_j + r)^d, \gamma > 0$.

- Radial Basis Function (RBF): $K(x_i, x_j) = \exp(-\gamma // x_i - x_j //^2), \gamma > 0$.

- Sigmoid: $K(x_i, x_j) = \tanh(\gamma x_i^T x_j + r)$.

Here, γ, r are kernel parameters.

4. Results and Discussion

Jefrries Matusita index that was tested for ROIs separabilities showed that all of the classes had good separabilities (>1.90), which is shown in Table (2). Therefore, the samples have a low correlation with each other, and many of the samples are not correlated at all, which indicates the high accuracy of the training samples taken for image classification. The panchromatic and multispectral bands of OLI sensor were fused based on FFT-PCA method. Figure (2), shows the result of OLI bands fusion with FFT-PCA method.

Table 2. Results of Jefrries Matusita index on ROIs correlation

	Water bodies	Snow	Rich range land	Poor range land	Agriculture	Fallow	Bare	settlement
Water bodies		2	2	2	2	2	2	2
Snow	2		2	2	2	2	2	2
Rich range land	2	2		1.99	1.99	1.99	1.99	2
Poor range land	2	2	1.99		2	2	1.97	2
Agriculture	2	2	1.99	2		1.93	2	2
Fallow	2	2	1.99	2	1.93		2	2
Bare	2	2	1.99	1.97	2	2		1.99
settlement	2	2	2	2	2	2	1.99	

Figure 2. Fusion of OLI panchromatic and multispectral bands based on FFT-PCA method

Three dimensionality reduction algorithms (PCA, ICA, MNF), were applied on the fused image to evaluate the effect of this algorithm on classification accuracy. The classification of images based on FFT-PCA-PCA, FFT-PCA-ICA and FFT-PCA-MNF methods was performed using a Support Vector Machine (SVM), algorithm with a radial kernel. Figures (3-5), show the classification result of images based on each dimensionality reduction algorithms.
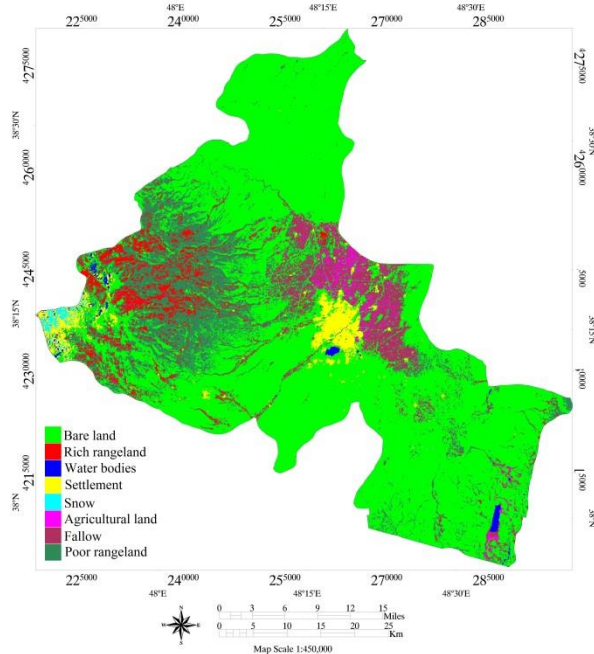
Figure 3. FFT-PCA-PCA based radial SVM classification
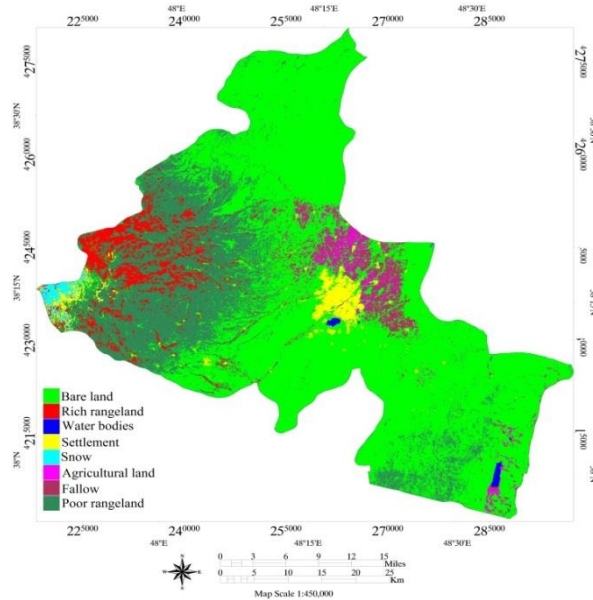
Figure 4. FFT-PCA-MNF based radial SVM classification
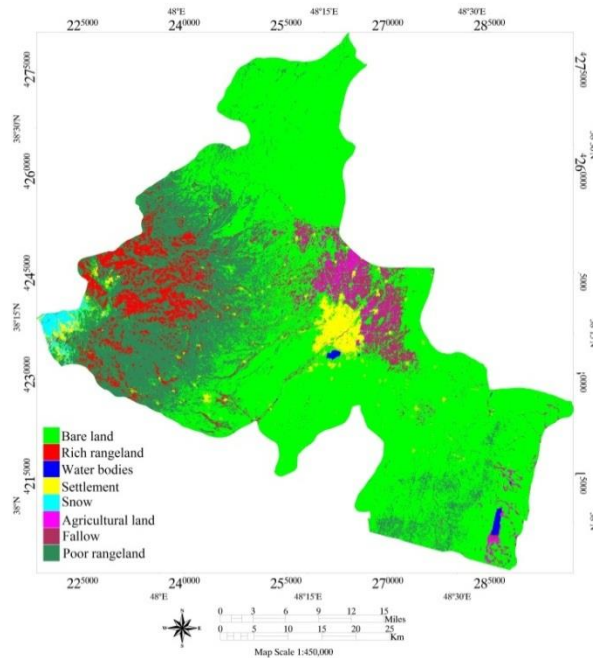
Figure 5. FFT-PCA-ICA based radial SVM classification

The results showed that FFT-PCA-ICA method have the lowest accuracy among the other two. This method has 86.9% and 0.84 overall accuracy and Kappa coefficient respectively. Also FFT-PCA-PCA method has an overall accuracy of 89% and Kappa coefficient of 0.91. The FFT-PCA-

MNF method has the highest accuracy among the other two DR methods in OLI data classification and has 96.8% and 0.96 overall accuracy and Kappa coefficient respectively. Table (3) shows the accuracy assessment of DR methods classification.

Table 3. Overall accuracy and Kappa coefficient

	Overall accuracy (%)	Kappa coefficient
FFT-PCA-ICA	86.9	84
FFT-PCA-PCA	89	91
FFT-PCA-MNF	96.8	96

Produce accuracy and user accuracy of DR methods based classification is shown in Table (4).

Table 4. Produce accuracy and User accuracy

		Prod. Acc(%)	User Acc(%)		Prod. Acc(%)	User Acc(%)		Prod. Acc(%)	User Acc(%)
	Bare land	80.43	51.39		100	86.67		97.44	97.44
	Rich rangeland	71.70	95		100	95		100	95
ICA	Water bodies	94.64	96.36	**PCA**	100	100	**MNF**	100	100
	Settlement	100	95		65	100		98.25	100
	Snow	98.72	96.25		100	69.37		100	100
	Agricultural land	75.81	87.04		100	92.73		92.16	87.04
	Fallow	72.37	84.62		93.55	100		88.71	93.22
	Poor range land	95.56	89.58		84.44	100		95.56	97.73

5. Conclusions

This paper has shown the FFT-PCA-DR based image classification accuracy assessment based on OLI data. The performance of SVM classification based on dimensionality reduction algorithms was quite good on OLI data classification. The overall accuracy and Kappa coefficient values range from 86.9% to 96.8% and 0.84 to 0.96 respectively, showed the effect of selected methods on final classification accuracy. Most of the classes are better classified when MNF DR method selected to SVMs input. The better noise reduction in MNF method may account for the better performance of an OLI data classification. Among the PCA and ICA methods, the ICA has a low performance because of its non-Gaussian nature that developed for hyperspectral data. In comparison to the related research (Lou et al., 2016; Sahisi and Krishna; Bashirpour et al., 2017), in this study, in addition to comparing three common methods of reducing data dimensions, a hybrid method has also been used to integrate data in order to increase the accuracy of data extraction from OLI data. In most studies conducted in this regard, the PCA, ICA, and MNF methods are used for hyper

spectral data that comparison of these three methods to multi-spectral data along with the FFT-PCA method is the strength of this research and distinguishes it from consistent researches.

References

Abbasi, B., Arefi, H., Bigdeli, B., & Roessner, S. (2015). Automatic generation of training data for hyperspectral image classification using Support Vector Machine. 36th International Symposium on Remote Sensing of Environment, Berlin, Germany.

Alhirmizy, S. A. (2015). Comparative Study between Landsat-8 OLI and Landsat-7 ETM+ for sensor signal-to-noise performance, Spectral Distortion, and spectral signature matching: A Study in the IRAQ Landscape, Remote sensing.

Arslan, O., Akyurken, O., & Kaya, S. (2017). A comparative analysis of classification methods for hyperspectral images generated with conventional dimension reduction methods. Turkish Journal of Electrical Engineering & Computer Sciences, 25, 58-72.

Asiedu, L., Adebanji, A. O., Oduro, F. T., & Mettle, F. O. (2016). Statistical assessment of PCA/SVD and FFT-PCA/SVD on variable facial expression. British journal of Mathematics & Computer science, 12, 1-23.

Bai, L., Xu, Ch., & Wang, C. (2015). A review of fusion methods of multispectral image. International Journal for Light and Electron Optics, 126, 4804-4807.

Bashirpour, M., Valadan Zoej, M. J., & Maghsoudi, Y. (2017). Effect of different SRFs on time series of spectral indices, between sentinel-2 and other sensors for the purpose of vegetation land cover monitoring. Journal of geospatial information technology, 5, 123-140.

Chul ko, B., Hun Kim, H., & Yeal Nam, J. (2015). Classification of potential water bodies using Landsat-8 OLI and combination of two boosted random forest classification. Sensors, 15, 13763-13777.

Dhavan, R., & Garg, N. K. (2014). A hybrid approach of wavelets for effective image fusion for multimodal medical images. International journal of technical research and application, 2, 44-48.

Ghasemlounia, R., & Sedaghat Herfe, N. (2017). Study on groundwater quality using geographic information system (GIS), Case study: Ardabil, Iran. Civil engineering, 3, 779-793.

Hasani Moghaddam, H., Adli Atiq, R., Gholami, J., Abasi Ghadim, M., & Zeaiean Firooz Abadi, P. (2018). Performance Analysis of Support Vector Machine, Neural Network and Maximum Likelihood in Land use/cover Mapping and GIS. 2nd International Conference on New Horizons in the Engineering Science, Yildiz Technical University. Istanbul. Turkey.

Hasani Moghaddam, H. (2017). Performance evaluation of wavelet transform with decision level algorithms in fusion of Hyperspectral and High spatial resolution images. MA thesis of Kharazmi University, Tehran. Iran.

Hsu, C. W., Chang, C. C., & Lin, C. J. (2003). A practical guide to support vector classification.

Kaur, D. (2016). Image fusion using Hybrid techniques (PCA+SWT). International journal of engineering and computer science, 5, 15661-15667.

Knight, E, J., & Kvaran, G. (2014). Landsat-8 operational land imager design, characterization and performance. Remote sensing, 6, 10286- 10305.

Kwak, N., & Kim, C. (2006). Dimensionality reduction based on ICA for regression problems, In International Conference on Artificial Neural Networks Springer, Berlin, Heidelberg.

Kumar Singla, S., Dev Garg, R., Prakash Dubey, O., & Bala, A. (2018). Extraction of crop information from reconstructed Landsat data in Himalayan Foothills region. 6th International Conference on smart computing and communication, Kurukshetra. India.

Lou, G., Chen, G., & Tian, L. (2016). Minimum Noise Fraction versus Principal Component Analysis as a Preprocessing Step for Hyper spectral Imagery Denoising. Canadian Journal of Remote Sensing, 42.

Liu, J. (2017). Application of satellite image time series and texture information in land cover characterization and burned area detection, Academic dissertation, University of Helsinki.

Mamachan, P., & Baby, J. (2015). Denoising of images using a hybrid image fusion algorithms. International journal of advanced research in electrical, electronic and instrumentation engineering, 4, 5813- 5818.

Ping, P., Zhu, X., & Wang, L. (2017). Similarities/ Dissimilarities arities analysis of protein sequences based on PCA-FFT. Journal of biological systems, 25, 29-45.

Qiu, F., Abdelsalam, M., & Thakkar, P. (2006). Spectral analysis of Aster data covering part of the Neoproterozoic Allaqi- Heiani suture, southern Egypt. Journal of African Earth science, 44, 169-180.

Sahisi, V. S., & Krishna, I. V. M. (2016). Performance evaluation of dimensionality reduction techniques on CHRIS hyper spectral data for surface discrimination. Journal of Geomatics, 10.

Sorzano, C. O. S., Vargas, J., & Montano, A. P. (2014). A survey of dimensionality reduction techniques, arXiv preprint arXiv:1403.2877.

Torahi, A., Adli Atiq, R., & Hasani Moghaddam, H. (2016). Evaluating the capability of supervised classification algorithms in land use/cover map preparation. The 1st national conference on geospatial information technology, K. N. Toosi University. Tehran. Iran.

Unlusoy, D. (2013). Image fusion for improving spatial resolution of multispectral satellite images, Thesis for Master of Science, Middle East technical university.

Varshney, P. K., & Arora, M. K. (2004). Advanced image processing techniques for remotely sensed hyperspectral data. Springer. USA.

Vivekan, A. J., Thirumurugan, P., & Dhanarega, A. J. (2014). Image fusion and improving classification accuracy: A review. International journal of engineering science & research technology, 3, 496-500.

Wang, J., & Chang, Ch. I. (2006). Independent Component Analysis-Based Dimensionality Reduction with Applications in Hyperspectral Image Analysis. IEEE Translation and geoscience and remote sensing, 44, 1586-1600.

Wang, M., Yu, J., Niu, L., & Sun, W. (2017). Unsupervised feature extraction for hyper spectral images using combined low rank representation and locally linear embedding, ICAASP, 1428-1431.

Yusuf, Y., Tetuko Sri Sumantyo, J., & Kuze, H. (2013). Spectral information analysis of image fusion data for remote sensing application. Geocarto international, 28, 291- 310.